ABSTRACT

Commissioning the Front-End Electronics for the CMS Hadron Calorimeter Upgrade

Adryanna Smith

Director: Jay R. Dittmann, Ph.D.

In the spring of 2015, the Large Hadron Collider (LHC) at CERN outside Geneva, Switzerland, began a new era of operation at a proton-proton collision energy of 13 TeV. To optimize the data gathered from collisions at higher beam energies and intensities, the Compact Muon Solenoid (CMS) detector is scheduled to be upgraded beginning in December 2017. We worked to characterize and calibrate the new front-end electronics, which include charge integrator and encoder (QIE) cards, for the CMS Hadron Calorimeter (HCAL). These electronics are necessary to extract more precise timing data and to combat the signal degradation observed over time due to radiation exposure. We tested over 700 QIE cards for direct shipment to CERN, where they have been assembled into readout modules and await installation. Results from the test suite show reliable performance in the QIEs and promising improvements over current detector technology.

APPROVED BY DIRECTOR OF HONORS THESIS:

_____

Dr. Jay R. Dittmann, Department of Physics

APPROVED BY THE HONORS PROGRAM:

_____

Dr. Elizabeth Corey, Director

DATE: _____

COMMISSIONING THE FRONT-END ELECTRONICS FOR THE CMS HADRON CALORIMETER UPGRADE

A Thesis Submitted to the Faculty of

Baylor University

In Partial Fulfillment of the Requirements for the

Honors Program

By

Adryanna Smith

Waco, Texas

May 2017

TABLE OF CONTENTS

LIST OF FIGURES

ACKNOWLEDGMENTS

After four years studying within the Baylor University Honors Program, one ought to take a long moment to reflect on the impact of such an experience. The thesis project, I believe, serves as a just symbol of those years. It allows me to show gratitude towards the physics department, especially its professors Dr. Jay Dittmann—my tireless, ever-helpful, and delightful mentor and advisor—and Dr. Kenichi Hatakeyama—my intro physics teacher who saw in me a curious mind towards the world of particle physics. It allows me to recognize the mentorship, leadership, and friendship that is modeled throughout the Baylor High Energy Physics group at large. It allows me to dote on the fascination I have towards the written word, coding languages now included. And furthermore, this project allows me to testify that everything indeed has its season: There is a time for writing a thesis and a time for kissing it adieu.

I would also like to acknowledge Dr. John Davis for the ways he has shaped my perception of science and mathematics through the Crane Scholars Program and for his willingness to participate on my defense panel. A special appreciation is due the US Department of Energy and the National Science Foundation, which have funded this research and many more projects within high energy physics. And lastly, I would like to express gratitude towards my parents and friends for their years-long support, encouragement, and love.

Pour la rose qui fait important le temps qu'on perd

CHAPTER ONE

Introduction to Particle Physics and the Standard Model

Through everyday experiences, the everyday man comes to know a version of physical reality that is at once laughably small and strangely vast. For millennia, we measured time leisurely in sun-dialed swaths. Measures of distance were limited at the lower scale by human sight, at the upper scale by little more than imagination. With no tangible need to engage with objects beyond these bounds of reality, we levied resources towards projects of agriculture, philosophy, engineering, medicine, and trade. In true human style, these projects blended curiosity, innovation, and diligence to advance a common goal. The talents for exploring and cultivating the world came naturally to man, and thus man applied his ingenuity to these ends.

Philosophical minds have been devising explanations and categories for the physical world since ancient times: Empedocles' four elements of nature, Democritus' indivisible *atomos*, and Aristotle's influential (yet flawed) descriptions of motion and matter, among others. However, the Renaissance brought a shift in the way knowledge of the physical world was put forward. The works of Copernicus, Galileo, and Kepler, who relied upon observations and mathematics to defend their models, led in this shift. To make informed observations, they demanded technological and theoretical innovation. The advent of the telescope and elliptical planetary motion attest to the fruitfulness of the emerging scientific approach. Inductive reasoning—the process of drawing probable conclusions based upon empirical evidence—offered a scaffold that aspiring scientific minds could scale with hypotheses and investigation.

This way of using reason to systematically explore physical reality prompted a stream of fresh insights, and the successes gave science a revolutionary position of influence, a position retained into the modern day. While astronomical progress

was being made to understand the heavens, 17th century advancements in microscopy illuminated another sphere of activity invisible to the naked eye. Fields using scientific inquiry began to develop distinct identities with tailored methodology, instruments, and goals. Between biology, chemistry, astronomy, and Newtonian physics, the levels at which we experimented and inquired extended further than ever before. Everyday humans were seated within an interesting middle ground, capable of using tools and ingenuity to probe the scales most foreign to daily life. For the purposes of this thesis, we will be interested in efforts to understand the world of the very tiny and fundamental.

1.1 A Curated Look at Particle Physics

Particle physics attempts to describe matter at its most basic level: the elementary particles that comprise it and the fundamental forces that govern how these particles relate. Just as all living things are comprised of more fundamental units called cells, all matter can be broken into atoms, the smallest piece of material which retains a chemical identity. Over the last century, scientists have demonstrated the existence of even smaller pieces of matter. These pieces, or particles, are believed to be elementary, and cannot be further broken down. These tiny particles and the interactions (or forces) between them are set out in a tremendously successful theory known as the Standard Model. As a field, particle physics may seem obscure, but its applications are indeed familiar and far-reaching.

The field credits its beginnings to J.J. Thomson's 1897 discovery of the electron. Thomson concluded that this new particle—far lighter than the lightest atom, hydrogen, and thus "subatomic"—also carried the negative charge that runs through electric wires. The following decade, the Rutherford scattering experiment fired small alpha particles at gold foil. When the alpha particles were deflected at large angles, the results provided unexpected empirical evidence that atoms had dense, positive cores. These cores were called nuclei and any further substructure remained unknown.

Meanwhile, the work of theorist Max Planck to resolve a thermodynamic curiosity known as the ultraviolet catastrophe led to the revolutionary notion that energy was quantized. Though energy levels seemed continuous at classical limits typical of the observable world, Planck demonstrated that energy must be transferred in small discrete units hf, where h is Planck's constant and f is the frequency of the harmonic oscillator. Planck's mathematical conclusions formed the basis of quantum theory and knocked down the first domino in a long chain of challenging results the 20th century had to reconcile. Physicists more than ever would need open dialogue between theory and experiment if they were to navigate the so-called quantum revolution.

After Einstein's "miracle year" of 1905, the theory of special relativity established that the speed of light alone was constant throughout the universe and that space and time measurements were subservient to the observer's reference frame. Furthermore, light itself was quantized into units (now called "photons"), which could be treated as both a particle and a wave. This wave-particle duality led to de Broglie's proposal that all matter possessed wave-like properties such as frequency and dispersion. Heisenberg put forth his famous uncertainty principle in 1927, introducing another complex result which, at face value, seemed absurd: the more precisely one measures a particle's speed, the less precisely one can measure its position, and vice versa. The same held for a particle's energy and time. Such a result bore no parallel within classical physics. Other theorists began constructing a formalism to handle the implications for both quantization and wave mechanics. Quantum mechanics was taking shape boldly along contemporary experiments exploring the nature of the electron, photon, and nucleus. Advances in nuclear study demonstrated the existence of positively charged protons and neutrally charged neutrons, both of which were given the umbrella term "nucleons."

As the decades advanced, particles of all sorts began emerging from experiments. The electron, proton, neutron, and photon were not alone. A relative to the

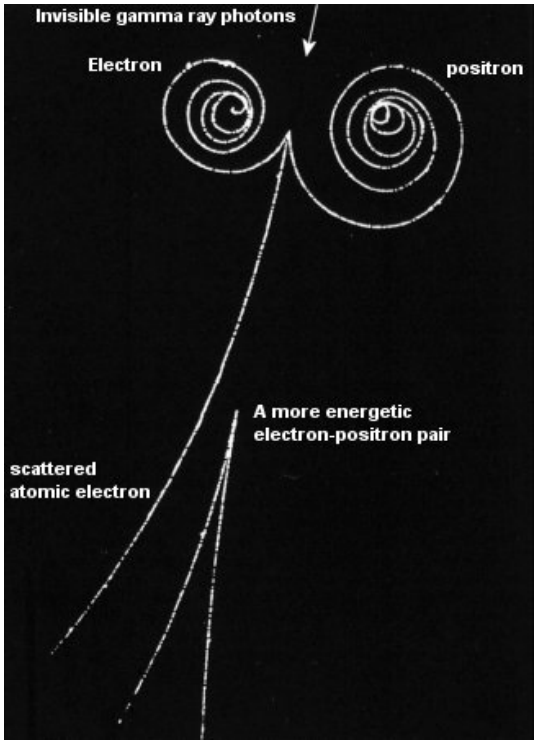

Figure 1.1. Example of positron-electron production in cloud chamber, a experimental signal that confirmed the existence of antiparticles [1]. The first recorded observation of an antiparticle was in 1932 by Carl Anderson. He would win the Nobel Prize in Physics four years later for the discovery of the positron.

electron, the "muon," was detected, and anomalies in observed processes led to the postulation of another particle, the traceless "neutrino." Antiparticles, which share the same mass as a particle but with the opposite charge, also emerged. At first mere by-products of the mathematics, they were spotted shortly thereafter in detectors called cloud chambers. Cloud chambers, one early apparatus used by physicists, are built of gaseous compartments that generate trails of mist when traversed by ionizing particles (Figure 1.1). Momentum and charge can be determined by exposing the chamber to a constant magnetic field and examining the curve of particle trajectories. Oppositely-charged particles spiral in reverse directions, and the identity of passing particles can be partially deduced by the width of the track. By the 1950s, detector technology upgraded to include bubble and spark chambers.

However, the cosmic rays that these experiments relied upon to generate events did not interact at a rate or energy feasible for the observation of certain rare phenomena and massive particles. An incident particle with higher kinetic energy has a smaller wavelength and can be used to probe even tiny targets with greater precision. To better control these factors, cyclotrons were developed in the 1930s and were then surpassed by synchrotron accelerators. The synchrotron utilizes an electric field of variable frequency that propels a beam of charged particles up to higher speeds (and therefore energies) while the beam circulates at a constant radius. This variable field means the synchrotron can accommodate particles moving at relativistic speeds, and thus became an attractive choice for particle accelerators.

While emerging technologies improved the capacity of accelerators and associated detectors, the data began pointing in interesting new directions. Precision measurements of scattering experiments hinted that protons and neutrons were not, in fact, elementary. The quark model therefore developed as a response to nucleons' composite nature. More progress was also being made on the front of unifying electromagnetic and weak interactions. Intent on pursuing these questions more thoroughly and at higher energies, scientists proposed a new machine to accelerate proton beams to nearly the speed of light. With a long line of predecessors paving the way, the Large Hadron Collider (LHC) situated outside Geneva, Switzerland, assumed operations in 2008.

1.2 Setting the Standard

Developed over the last 50 years, the Standard Model (SM) is the most unified theory that particle physicists have to explain particles and their subatomic behavior. The model is a result of careful experiment and brilliant theoretical interpolation and states that the fundamental forces themselves are mediated by exchange particles. In this view, particles are classified into two types: those which make up the material world, and those which facilitate interactions within it. Particles of the first type are

called "fermions," and of the second, "bosons." The discovery of the Higgs boson, announced July 4, 2012 at the LHC, was the most recent success of the theory and, in many ways, the capstone find for SM physics.

The fermions are a collection of 12 elementary particles (plus their respective antiparticles). All fermions share the property of non-integer spin, and therefore abide by the Pauli exclusion principle. Based on SM properties like charge and color, fermions are further divided into families known as leptons and quarks. Both leptons and quarks are understood to exist in three "generations," each generation tending to contain more massive particles than the last.

There are six quarks, each denominated by its own "flavor." They are presented here in their generational pairs: the up and down quark, charm and strange quark, and top and bottom quark. Within each generation, the leading quark has electric charge $+2/3$, and the latter has $-1/3$. Quarks have their own special property known as color, which physicists traditionally label red, blue, or green. Antiquarks take on anti-red, anti-blue, or anti-green. Composite particles that are made of quarks are known as hadrons, and all hadrons by necessity are organized to be color-neutral. Nucleons are the two most familiar types of hadrons: protons are built from two up quarks and one down, while neutrons are built from one up quark and two downs. The top quark, discovered in 1995 at the Fermi National Accelerator Laboratory, is another noteworthy character, having the largest mass of all fundamental SM particles. In fact, it is nearly 40 times heavier than the next-lightest quark. For this reason, the top quark couples to processes that are important to current research ambitions, such as those involving the Higgs boson.

The overarching feature of the quarks is their participation in the strong force, which is the most powerful of the four fundamental forces. It is responsible for confining quarks into hadrons and nucleons into nuclei and is mediated by the exchange of gluons, one of the gauge bosons. Though powerful, the strong force has an incredibly

short range—roughly the size of a nucleon, only 10^{-15} m. These features have an interesting consequence. The amount of energy necessary to pull a quark away from other quarks to which it is bound outstrips the energy threshold for pair production. This produces new quarks which simply bind afresh, meaning an isolated quark has never been experimentally observed. The theory behind the strong force is known as quantum chromodynamics (QCD), named for the role that color plays in quark-gluon interactions.

Just as there are six quarks, there are six leptons. The leptons do not interact via the strong force and are therefore colorless. The leptonic generations, or "flavors," follow a naming scheme based on the particles themselves: the electron and its electron neutrino, muon and muon neutrino, and tau and tau neutrino. The neutrinos, as their name implies, are electrically neutral and carry no charge. They find their charged partner in the other leptons, all of which carry an electric charge of -1. Neutrinos were presumed massless until recent experiments confirmed the phenomenon of neutrino flavor oscillation. In such oscillations, ultra-light neutrinos change from one flavor to another during flight, necessitating a framework of mass eigenstates. Because neutrinos are neutral and light, they pass almost imperceptibly through most detectors and consequently are one of the least understood elementary particles.

While the fermions taken as a whole make up all of matter, only three of the particles actually comprise the atoms of the visible universe. The sufficiency of the up quark, down quark, and electron—all members of the first generation of fermions—calls into question the purpose of their more massive, unstable cousins.

The bosons are the fermions' compatible helpmates, set apart by their integer spin. Gauge bosons act as force carriers and the Higgs boson gives particles mass. Predicted in the 1960s and remaining hidden for half a century more, the Higgs boson was the final particle anticipated by the SM. The landmark discovery planted

the Higgs mass around 125 GeV/c^2 and was significant in delivering a boson whose associated mechanism explained why elementary particles have mass at all. Three of the SM gauge bosons owe their mass to this Higgs. These three, the $W^{\pm}$ and Z^0, are the exchange particles for the weak force, possessing electric charges of ± 1 and 0, respectively. The weak interaction governs radioactive particle decays, and without these bosons, one type of particle could not transform into another—the foundation of collider physics. Therefore, the $W^{\pm}$ and Z^0 play a particularly prevalent part in the rich complexities of modern particle physics. The remaining two gauge bosons, the gluon and photon, are massless and possess no electric charge. The gluon mediates the strong nuclear interaction and, since it carries color itself, participates in the interaction as well. The photon is responsible for the perpetuation of the electromagnetic field, affecting only those particles that carry charge. The field can act either to repulse or attract different particles, depending on this charge. From radio waves to friction to the stability of the atom, the electromagnetic force is familiar and, like gravity, extends over an infinite range. Similar to the strong force, a theory called quantum electrodynamics (QED) is the standard used to describe this interaction.

1.3 The Great Beyond

Though the SM's success lies in how accurately it both describes and predicts experimental data, the decades-long search for the Higgs was the last prediction to verify. Physicists have long known that there are deficiencies in the theory and that new models must emerge as the journey to understand continues. These models search for physics beyond the Standard Model. For instance, the current framework presumed massless neutrinos, which the observation of neutrino oscillations then adjusted. There is also the SM's failure to provide a suitable dark matter candidate; neither can it account for CP violation, an example of symmetry breaking which gives rise to the disproportionate matter-antimatter ratio observed in our universe. Perhaps most glaring is the lack of incorporation of the graviton, the theorized exchange

particle for the force of gravity. One of the chief aims of the LHC and of physicists across the globe is to analyze the data and brainstorm new approaches in an effort to leap beyond the sturdy framework and inch one step closer to the underlying principles of our world.

CHAPTER TWO

The Large Hadron Collider and Experimental Detectors

Tasked with understanding the properties, quirks, and realities of the subatomic sphere, thousands of experimental physicists turn to advanced detector technologies to study complex interactions between subatomic particles. In the pursuit of this study, robust machines must be built to accelerate small particles to tremendous energies to produce the massive particles central to current theories. One powerful implication of Einstein's mass-energy equivalence principle $E = mc^2$ holds that high-energy protons can collide to produce particles with rest masses far greater than that of the incident particles. By understanding these derivative particles in each collision, we validate current physical models and make new discoveries. With these principles in mind—and over several decades—scientists have constructed particle colliders with diverse incident particles, daring detector designs, and ever-increasing energies. Indeed, the field has come to be known as high energy particle physics. The world's most energetic instrument to this end is the Large Hadron Collider, which will be, in tandem with its detectors, the subject of this chapter.

2.1 A Brief Look at Energy and Luminosity

Several key measurements help to characterize the performance of high energy physics technology and particle interactions. It is appropriate here to offer a brief explanation of three commonly used terms: the electronvolt, center-of-mass energy, and luminosity. Due to mass-energy equivalence, particle physicists often cite both energies and masses of particles in units of *electronvolt*, or eV. An electronvolt is the amount of energy transferred to an electron traveling across a potential difference of one volt. In reference to SI units, 1 eV equals approximately 1.0622×10^{-19} Joules. Aside from neutrinos, the electron is the lightest lepton, with

a rest mass of 0.511 MeV/c^2. The heaviest of the Standard Model particles is the top quark, with a rest mass around 172 GeV/c^2. Thus, to produce such particles in a collider, the collision energy must exceed this rest mass.

Measurement of this collision energy abides by special relativity considerations and is known as the *center-of-mass energy.* When two beams of particles strike head-on, the center-of-mass energy is found by summing the energies of the two oncoming particles, as observed by the center-of-mass frame of the collision. For a particle collider with two opposing proton beams, each at 6.5 TeV, the center-of-mass energy is denoted as $\sqrt{s} = 13$ TeV. This value is all the energy available to the interaction and subsequent decays.

To characterize a collider, it is also essential to measure the instantaneous luminosity, the number of particles per time per cross section in the beam line [3, 7]. The instantaneous luminosity is a physical quantity defined in simple terms to be:

$$\mathcal{L} = \frac{F \times f n_1 n_2}{4\pi\sigma_x\sigma_y}$$

where f is the frequency of collisions, n_1 and n_2 are the number of particles in each incoming bunch, σ_x and σ_y are the spans of the beam in the transverse directions, and F is a geometric reduction factor dependent upon the angle at which the two beams collide. Instantaneous luminosity has units of cm^{-2} s^{-1}. By integrating with respect to time, the integrated luminosity is calculated, canonically reported in units of inverse femtobarns, or fb^{-1}, where one barn is a unit of area equal to 100 fm^2, or 10^{-24} cm^2. These units and quantities are indispensable to an understanding of collider physics and inform benchmark parameters of machines like the LHC.

2.2 The Large Hadron Collider

2.2.1 An Overview

Operating 100 meters beneath the surface of the Franco-Swiss border, the Large Hadron Collider (LHC) is the most powerful particle collider endeavored to date. The proton-proton collider and its associated accelerator facilities are installed at the European Organization for Nuclear Research (CERN) just outside of Geneva, Switzerland. The design specifications for the LHC allow optimal performance at a center-of-mass energy $\sqrt{s} = 14$ TeV and instantaneous luminosity $\mathcal{L} = 10^{34}$ cm^{-2}s^{-1} [8].

After CERN's Large Electron-Positron Collider (LEP) was decommissioned in 2000, the 27-kilometer tunnel was refitted to accommodate the LHC and its aims of probing particle interactions at the TeV scale. The first stable proton beams of the new collider were achieved in 2008, and Run 1 operations peaked at 8 TeV before a scheduled shutdown in 2013. Since beginning Run 2 in April 2015, proton-proton collisions at the LHC generate a record center-of-mass energy $\sqrt{s} = 13$ TeV.

2.2.2 The Acceleration Chain at CERN

In order to accelerate protons to extreme energies at the LHC [9, 10], particles tour a chain of successively larger linear and circular accelerators (Figure 2.1). Gaseous hydrogen atoms are first stripped of their lone electron and delivered to the Linac2 linear accelerator. After leaving Linac2 at 50 MeV, the protons are pushed to 1.4 GeV in the Proton Synchrotron Booster (PSB) and are fed into the Proton Synchrotron (PS) ring, where they reach 25 GeV. In this stage, the continuous proton beam must be segmented into "bunches" of 4-ns length. Roughly 100 billion protons constitute each bunch. These bunches are spaced 25 ns apart to accommodate Run 2 LHC specifications. The Proton Synchrotron injects into the Super Proton Synchrotron (SPS), itself 7 km in circumference. The SPS accelerates proton

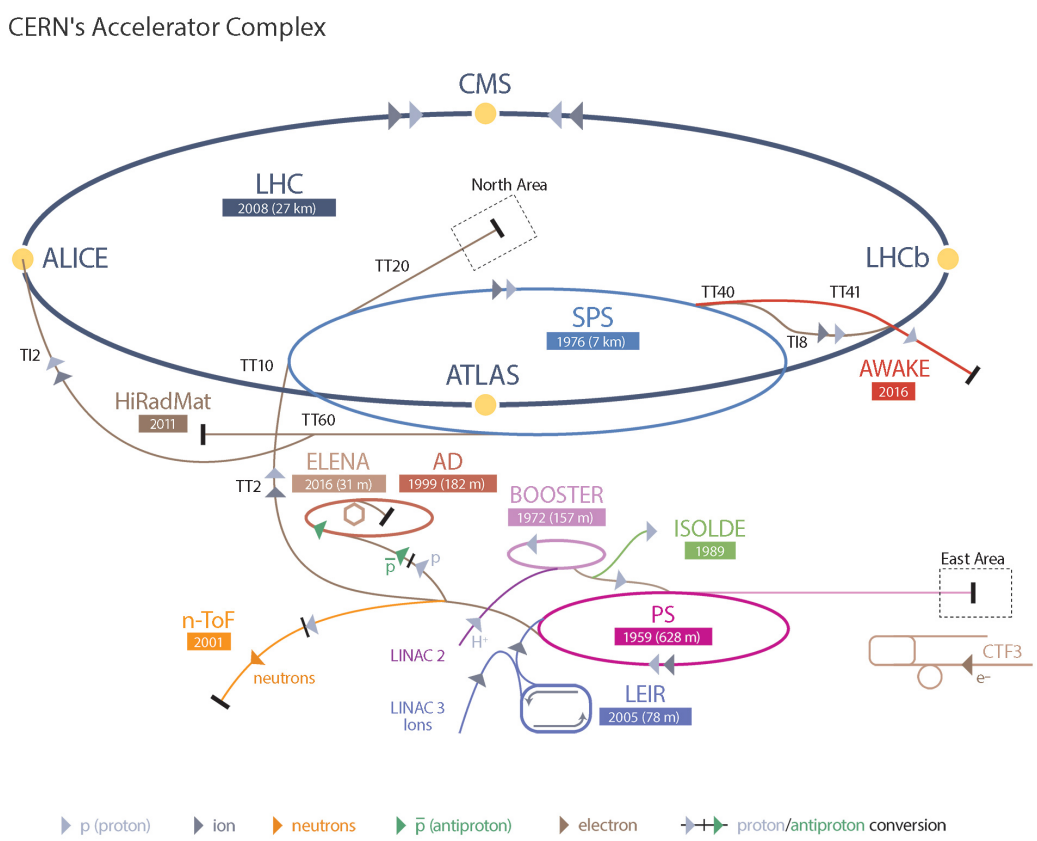

Figure 2.1. The accelerator complex at CERN

bunches to 450 GeV, after which point the beam splits and enters the two pipes of the LHC—one circling clockwise, the other, counterclockwise—for the final boost.

To this end, the LHC runs approximately 10^4 amperes of current through thousands of superconducting magnets. To sustain superconductive conditions, superfluid helium cools the system down to 1.9 K. A pattern of dipole and quadrupole magnets placed around the ring works to propel and focus the protons. Each beam achieves its final energy of 6.5 TeV after circulating 20 minutes in this largest ring [10], ensuring the desired 13 TeV upon collision. Protons at these energies have been propelled to just shy of the speed of light, 3×10^8 m/s.

2.2.3 The LHC Detectors

The unique and powerful design of the LHC affords access to a range of research as vast as it is precise. To capitalize on the highly energetic collisions, intensive planning and development were dedicated to the construction of detectors to fit around the beam line at major interaction points. Four interaction points are dotted along the main ring of the LHC, each hosting an independent detector (Figure 2.2). Two of the detectors, A Large Ion Collider Experiment (ALICE) and Large Hadron Collider beauty (LHCb), focus their investigations on phenomena in the areas of heavy-ion and b-quark physics, respectively. The two remaining major detectors, A Toroidal LHC Apparatus (ATLAS) and Compact Muon Solenoid (CMS), are multi-purpose detectors built to capture the wide spectrum of particle interactions with high precision. These detectors dissect Standard Model phenomena, robustly analyzing known decay modes and looking for clues as to what could lie beyond the current theory. Similar in scope and purpose, the CMS and ATLAS experiments are poised so that each independently corroborates the other's results, with the advantage that cross-checks strengthen both experiments' publications. Proton-proton collisions occur at these four detector halls when the two proton beams, circling in opposite directions about the ring, are crossed and squeezed together by a magnetic field. As bunches circulate in the LHC ring—up to 2,808 in each direction—collisions take place inside the detectors at a staggering 40 million times per second.

This high rate of collisions poses a significant design challenge to experimental teams seeking accurate event data. For each "bunch crossing" within a detector, dozens of collisions are expected due to high luminosity and the sheer number of eligible protons. This phenomenon—known as "pile-up"—introduces a significant challenge in determining which particles seen in the detector originate from which proton-proton collision. As a reference, during 8 TeV runs in 2012, CMS recorded an average of 21 interactions per bunch crossing, as seen in the Figure 2.3. Since higher

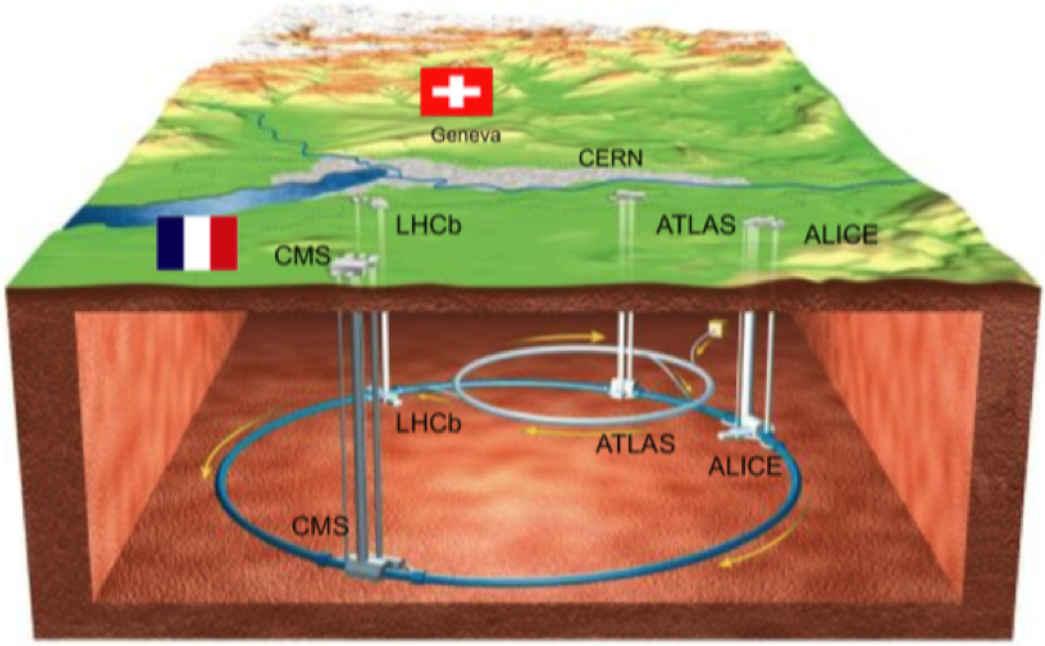

Figure 2.2. The LHC and four main experimental halls, situated underground the Franco-Swiss border outside of Geneva [2].

luminosities increase the statistical significance of results and improve the chance of seeing rare phenomena, high pile-up is a necessary side effect of efficient collider physics at this scale. The technology solutions that CMS utilizes to address pile-up will be discussed in a future section.

2.3 Compact Muon Solenoid

2.3.1 Overview of CMS

With ambitions to canvas as much of the interaction landscape as possible with precision down to the width of a human hair, the Compact Muon Solenoid (CMS) is one of two general-purpose detectors housed underground at the LHC. The CMS experiment is comprised of over four thousand scientists from nearly two hundred institutions across the globe. The 14,000-ton CMS detector itself is an enormous cylindrical apparatus that is 21 m long and 15 m in diameter.

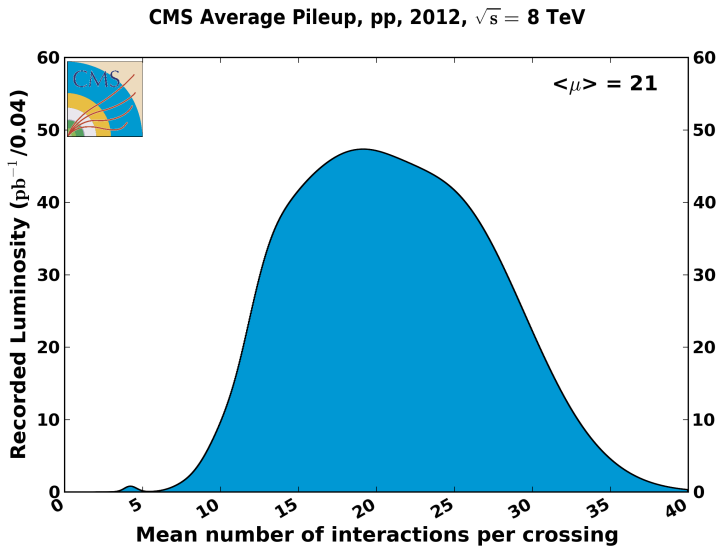

Figure 2.3. Integrated luminosity vs. interactions per bunch crossing, showing pile-up in CMS during 2012 operations at $\sqrt{s} = 8$ TeV.

Many subdetectors with their own specialized functions build up the onion-like layers of CMS (Figure 2.4) [3, 2]. The region of CMS closest to the beam line hosts systems to track the trajectory of charged particles and is surrounded by two layers of calorimetry which gather information on the energy of particles produced in the interactions. The powerful solenoid, within which these inner layers are snugly constructed, is the largest in the world and produces a magnetic field five orders of magnitude stronger than that of Earth. Hefty layers of steel and chambers built to detect long-living muons surround the solenoid, completing the structure of CMS and earning the detector its middle initial. Cursory treatment of each subdetector is given below:

- *Inner tracker*: comprised of pixel sensors and silicon trackers, charts the momentum of charged particles bent characteristically in the magnetic field
- *Electromagnetic calorimeter (ECAL)*: homogenous system of lead tungstate crystals; measures the energy of charged leptons and photons with fast response

- *Hadronic calorimeter (HCAL)*: configuration of brass absorber and plastic scintillator; measures the energy of hadrons (baryons, mesons) by initiating showers of secondary particles
- *Superconducting solenoid*: central, eponymous feature of CMS; delivers a 4-Tesla magnetic field via superconductive niobium-titanium coils, providing the necessary field strength for effective spectrometry in the inner tracker and muon chambers
- *Muon chambers*: system of resistive plates and cathode strips; identifies muons and their momenta with high spatial resolution
- *Return yoke*: steel structure woven around the muon system; operates a 2-Tesla magnetic field to aid muon detection and contain the solenoid's field

The trackers and calorimeters are complementary instruments necessary for the identification of both charged and neutral particles. Furthermore, the energy E resolution of calorimeters increases as $1/\sqrt{E}$, while that of spectrometers falls with E [11]. Taken as a whole, the detector works to counterbalance its own deficiencies in sensitivity. Data on momentum and energy are obtained by analyzing particle trajectory and light production in the calorimetric layers, partnering together in advanced online algorithms to relay the interesting collision data through to offline analysis.

2.3.2 CMS Coordinate System

For the purpose of event reconstruction and precise design requirements, CMS follows a right-handed coordinate system centered about the interaction point along the beam line [9]. The x-axis extends inward towards the center of the LHC ring and the y-axis extends upwards. Perpendicular to these, the z-axis then points along the beam line, counterclockwise. Given the symmetry of the detector, spherical coordinates (r, θ, ϕ) lend the most suitable variables. The polar angle θ and azimuthal angle ϕ are measured in the standard way from the z-axis and x-axis, respectively. The

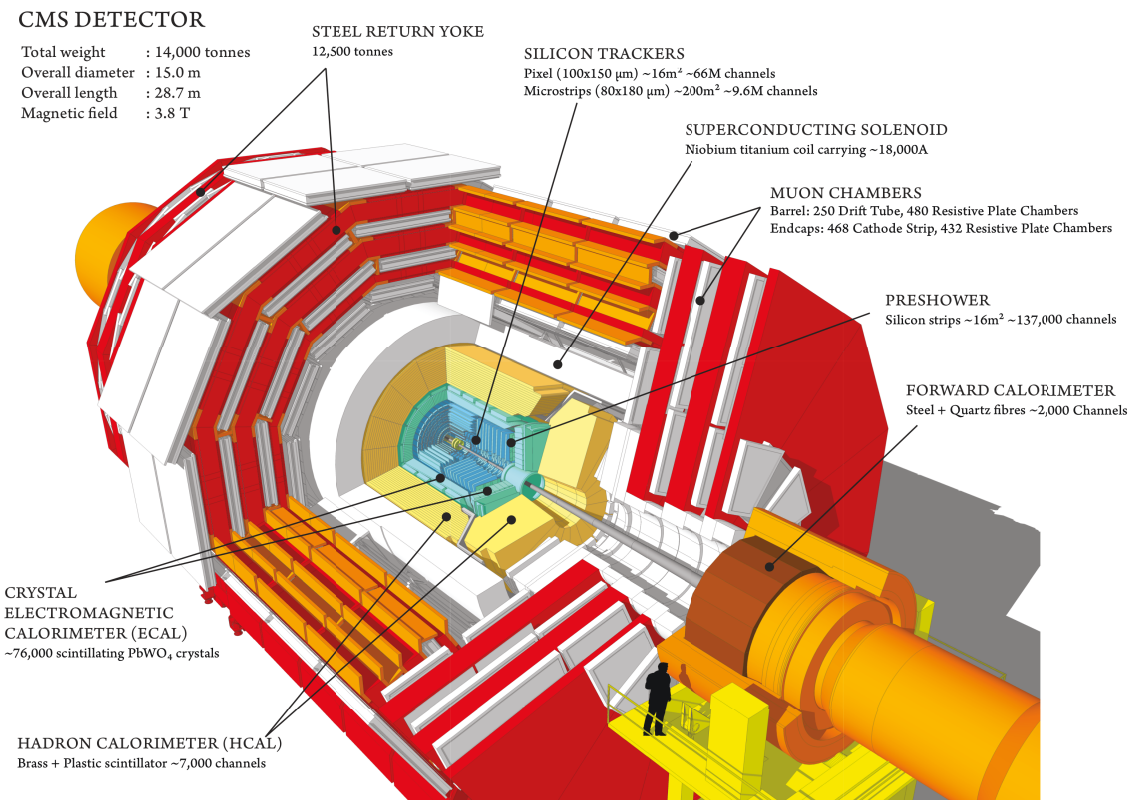

Figure 2.4. Cutout of the CMS detector, with a person for scale. The Hadron Calorimeter (HCAL), in yellow, is lodged directly between ECAL and the solenoid. Each subdetector wraps concentrically around the beam line, which extends down the center.

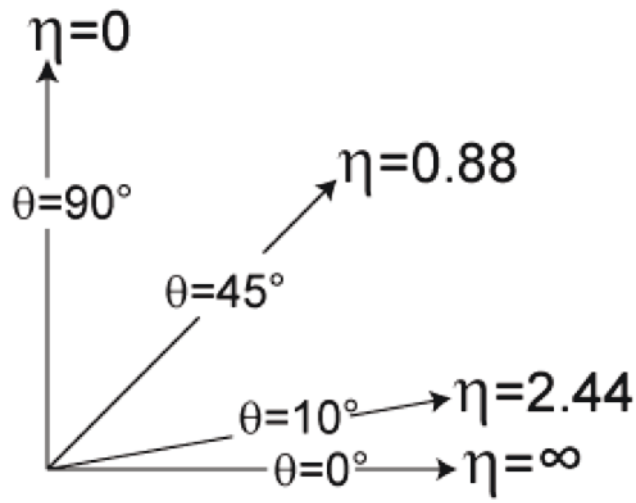

Figure 2.5. The relationship between η and θ, where the vertical axis represents the x-y plane and the horizontal axis is the z-axis directed along the beam line.

radial coordinate r extends outward from the origin. It becomes further preferred to define the angle from the beam axis in terms of a new variable for pseudorapidity, η:

$$\eta = -\ln\left[\tan\ \frac{\theta}{2}\right]$$

The quantity η is conveniently Lorentz-invariant for massless particles in the z-direction. As θ points parallel to the beam line, η tends to infinity (Figure 2.5).

2.3.3 The CMS Hadron Calorimeter

The Hadron Calorimeter (HCAL), situated just beyond the ECAL, is designed to measure the amount of energy that hadronic particles deposit. As a sampling calorimeter, it is distinct in its design from the entirely crystalline ECAL by alternating between layers of brass and plastic scintillator. The dense metal halts hadrons emerging from the inner layers of CMS, scattering these composite particles of quarks and gluons into secondary particles. In quick turn, showers of secondary particles deposit their energy into the layered scintillators, which generate light proportional to the amount of energy the particles possess. In this way, the detector sees a portion,

or "sample," of the total hadron energy via scintillation, with the rest absorbed by the metal. The readout of the signal begins with green wavelength-shifting fibers that carry scintillated light to HCAL's front-end electronics [12]. There, photodiodes convert light into electric current. Special integrated circuit chips known as Charge Integrators and Encoders (QIE) process the current, serializing both energy and timing information. With the signal broken into bytes, fiber optics carry the information to the back-end electronics to be buffered for the preliminary trigger and data acquisition (DAQ) stage. The entire process can operate at the 40 MHz collision rate of the LHC, corresponding to the 25 ns rate of bunch crossings within the CMS detector.

To facilitate resolution in the transverse direction, HCAL is divided into four distinct sectors with varying angular coverage and geometries (Figure 2.6) [3]:

- *Barrel (HB)*: covers $|\eta| < 1.3$, cylindrical design segmented into wedges, each composed of alternating brass and scintillator stacked outwards
- *Endcap (HE)*: covers $1.3 < |\eta| < 3.0$, disk design that promotes a nearly hermetic system
- *Outer (HO)*: covers $|\eta| < 1.3$, cylindrical design located outside of HB and the solenoid
- *Forward (HF)*: covers $3.0 < |\eta| < 5.2$, cylindrical design accommodating particles emerging from the detector quite close to the beam line

2.4 Upgrading the CMS Detector

The detectors at the most energetic particle collider in the world, despite the advanced technology and radiation hardness that factored in during their construction, are not immune to the daily irradiation and upward trends in energy and luminosity at the LHC. In anticipation of these changing conditions, the LHC is scheduled to perform runs interspersed with technical stops and shutdowns. These stops allow experiments like CMS to perform maintenance and upgrades to their detectors to accommodate damaged materials, innovations in technology, and updated collider

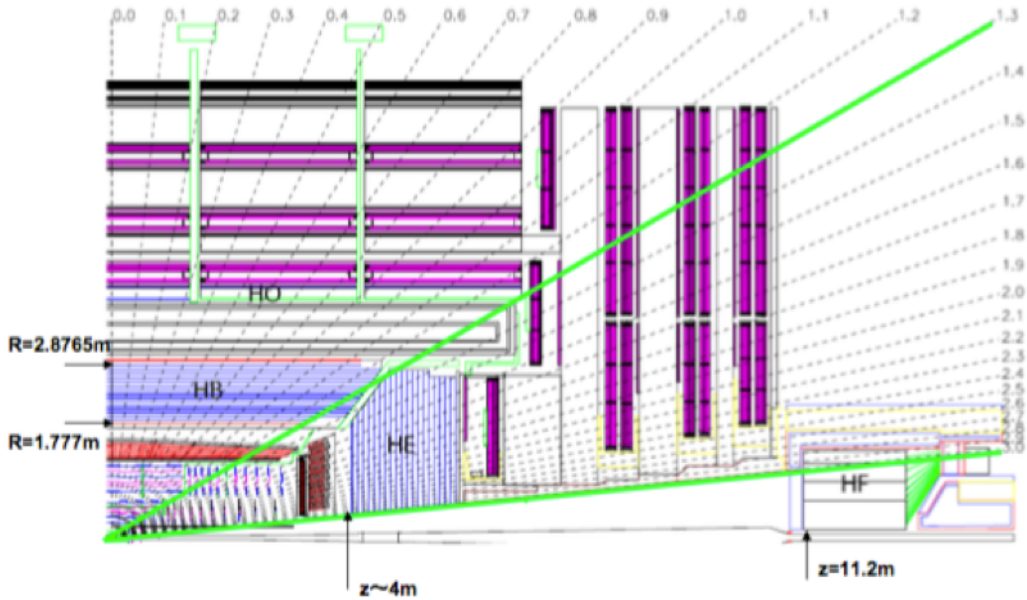

Figure 2.6. Longitudinal view of the four subsystems of HCAL with η projected onto the diagram. They achieve sensitivity up to $|\eta| \sim 5$; the non-contiguous placement of HF was necessary due to space limitations at the center of the detector [3].

conditions. Upgrades to CMS seek to improve features in HCAL such as response to pile-up, efficiency in signal readout, and depth resolution for identifying particles throughout the calorimeter volume.

After Run 1 of the LHC concluded in 2013 at 8 TeV, the LHC entered Long Shutdown 1 to prepare for proton beams at 13 TeV. Though R&D efforts towards the CMS upgrade were already underway, feedback from Run 1 indicated that the radiation damage done to HCAL's endcap (HE) exceeded predictions (Figure 2.7). The severe signal degradation from HE promoted studies into better understanding the effect of radiation dose and rate on materials used for scintillation and signal readout. The front-end electronics of HE are likewise poised for replacement. A new generation of QIE chips, called the QIE11, will be installed in an upcoming shutdown, along with new photodetector technology: the silicon photomultiplier (SiPM). The quality control and calibration efforts made over the summer of 2016 to commission the new front-end electronics will be the topic of this thesis.

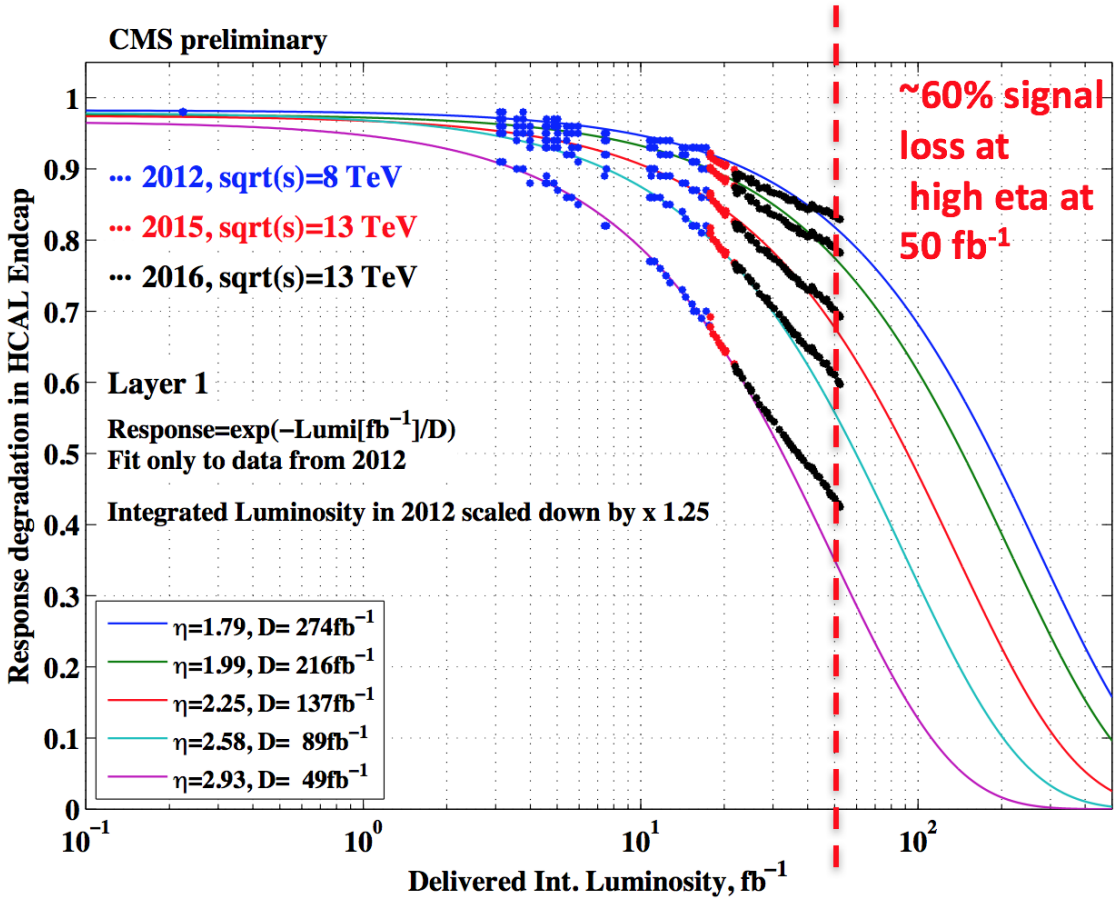

Figure 2.7. Signal degradation in HCAL HE vs. integrated luminosity in Run 1. Extending this trend to 3000 fb^{-1}, the value which HE must withstand throughout its lifetime, it is evident that current detector technology would be insupportable.

CHAPTER THREE

Quality Control and Calibration of HCAL Front-End Electronics

As discussed at the close of Chapter 2, scheduled technical stops in the operation of the LHC are periodically observed. During these technical stops, technicians, engineers, and physicists can enter the underground caverns where LHC detectors like CMS are housed and perform work on the machines. Aside from basic maintenance, this work can involve substantial upgrades to the design, electronics, and materials of the detector. Due to the tedious and ambitious nature of disassembly and reassembly of detector layers, such changes are only performed after extensive R&D. These efforts must demonstrate the reliability and improved performance of the upgrade.

The upgrade of HCAL's endcap readout electronics, initially slated for the technical stop in December 2016, required such R&D efforts. For our work during the summer of 2016, we created and performed necessary tests to verify and justify the installment of HE's new front-end electronics. The work was conducted at the Fermi National Accelerator Laboratory in Batavia, Illinois, the premier high energy physics facility in the United States.

The HE upgrade follows on the heels of HF's, the forward sector of HCAL. Both sectors suffered from anomalous signals in damaged photodetectors and both seek solutions for the LHC collision spacing of 25 ns. The updates in front-end electronics for HE are similar for HF. Due to the on-detector space constraints, there is also a need for compact materials and an electronics chain that interfaces to the back-end electronics, which are shared by many HCAL subsystems.

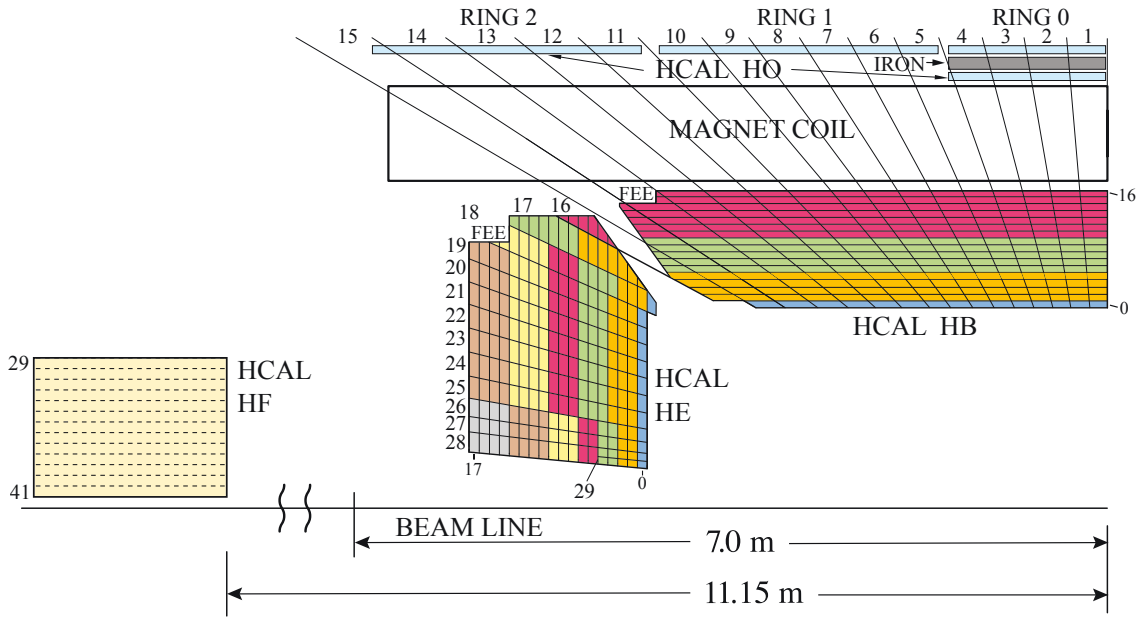

Figure 3.1. A scheme for the new depth segmentation in HCAL, viewed across the length of the detector. The figure shows one-fourth of HCAL, with the other fourths reflected symmetrically across the right-most vertical axis and across the beamline. The interaction point where the two proton beams collide is located in the lower right corner.

3.1 Hardware

3.1.1 Silicon Photomultipliers

In the original design of HE, the photodetectors of choice were hybrid photodiodes (HPDs). These HPDs receive the optical signal produced via scintillation and convert it to an electrical signal that can be processed by the front-end electronic chips. While the HPD technology has fast response and reasonably high gain, noise effects observed at the requisite high voltage of 8 kV and suspected photocathode drifting both indicated the need for new photodetector technology.

The technology elected for the HE upgrade is the silicon photomultiplier (SiPM), an avalanche photodiode (APD) operating in Geiger mode. The SiPM devices to be used in HE contain 2.8- and 3.3-mm-diameter round sensors, each comprised of an array of over 20,000 microcells. As a solid state device, the SiPMs are

robust and tiny compared to HPDs, enjoying a low bias voltage as well as an insensitivity to the strong magnetic field within the CMS solenoid. With gains up to 10^6—orders of magnitude larger than those of HPDs—and with the capability to respond at the single-photon level, the SiPMs deliver signals that far outpace detector noise. This favorable signal-to-noise ratio allows for higher-granularity response in the HCAL volume: by coordinating individual SiPMs with smaller clusters of scintillator tiles, the upgrade allows for previously unattainable depth segmentation (Figure 3.1). This new segmentation enhances physicists' ability to distinguish pile-up effects and to apply advanced particle-flow algorithms to event reconstruction.

3.1.2 QIE Cards

The Charge Integrator and Encoder (QIE) is the electronic chip designed to convert the analog pulse from the SiPMs into digital data. As an application-specific integrated circuit (ASIC), the features of the newest QIE chip have grown up around the unique needs of the CMS HCAL. The primary purpose of the chip is to process the calorimetry data in a speedy, precise, and digital way so that data can be transmitted efficiently down the electronics chain. To accomplish this, the chip integrates the input current pulse over a 25-ns window to calculate the corresponding amount of charge. This charge is then encoded by the analog-to-digital converter (ADC) in a clever way to conserve bits. Using a semi-logarithmic binning scheme, the ADC value is split into a 6-bit mantissa and a 2-bit exponent, which denotes one of four ranges (Figure 3.2). Thus, the ADC transmits only 8 bits—1 byte—for any given measurement with approximately 3-fC resolution up to 330 pC. This scheme retains the precision desirable at low charge input while also allowing the chip to respond well at high charge input.

The QIE11 chip improves upon its predecessor (QIE8) by introducing time-to-digital conversion (TDC) functionality. The TDC can record pulse arrival time and pulse width by splitting each 25-ns integration window into 50 bins of 500-ps

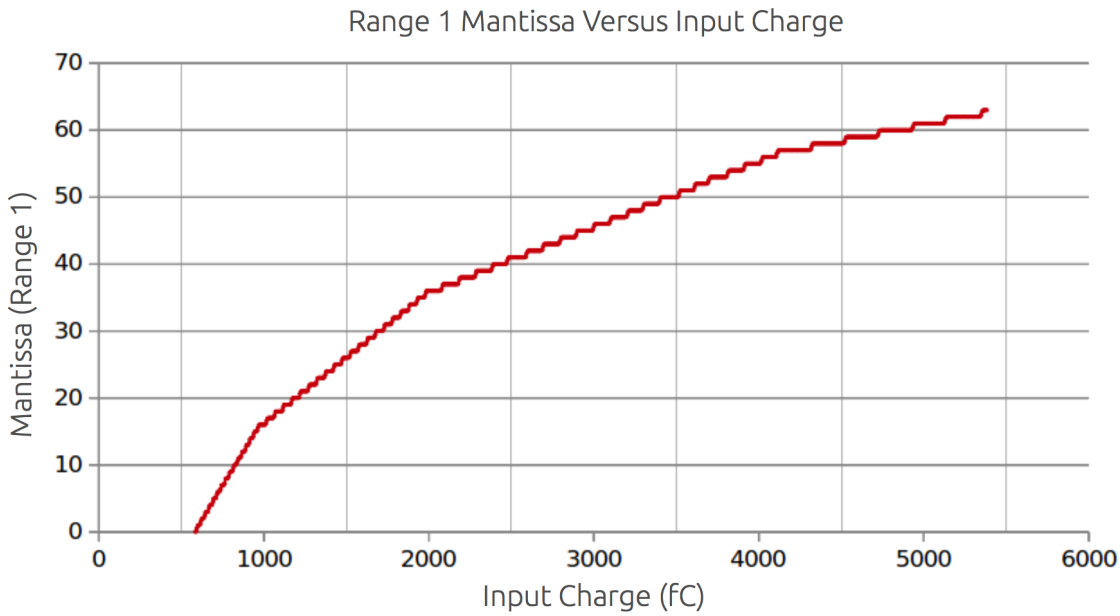

Figure 3.2. For range 1 (out of 0-3), an illustration of mantissa vs. input charge for a QIE chip's ADC functionality. Notice the 4 distinct subranges within this single range. These subranges and their varying slopes are canonical characteristics of proper QIE response [4].

width. Once an incoming current pulse crosses the preset threshold of the QIE, the TDC information is stored using a 6-bit code. This timing functionality allows better signal precision when proton bunches collide at 25 ns in Run 2 of the LHC. Thus, while the QIE's window of current integration remains fixed at 25 ns internally, the readout electronics will have the capability of distinguishing a pulse's leading edge within this window. The TDC feature is a desirable improvement in the environment of high event pile-up at high luminosity.

The QIE11 chips are arranged in two banks of 6 chips on a special circuit board called the QIE card (Figure 3.3). The twelve chips correspond to 12 channels, all of which send their digitized signal to one central field-programmable gate array (FPGA) on the card. This FPGA, the IGLOO2, formats the data from the chips and then sends it onward to the back-end electronics in one packet. Since the IGLOO2's internal registers record the instantaneous status of the QIE chips, accessing and examining

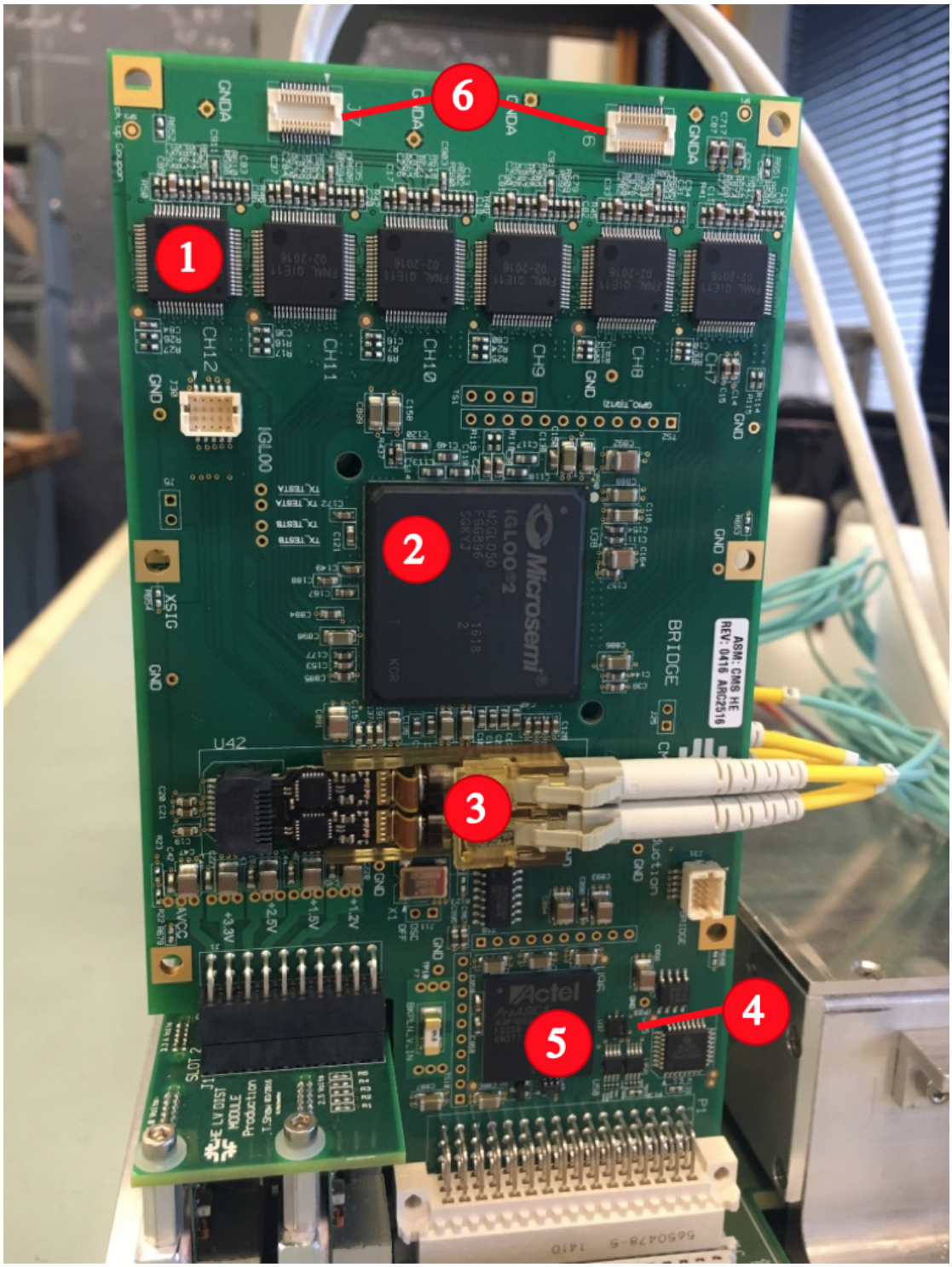

Figure 3.3. A QIE card slotted into the backplane. 1) Six QIE11 chips—on the reverse side of the card there are six more; 2) IGLOO2 FPGA; 3) VTTx housing with two optical links; 4) humidity and temperature sensor; 5) Bridge FPGA; 6) connectors for analog signal input

these registers was a crucial step in our work to ensure the chips were functioning properly. The data packet from the IGLOO2 leaves the QIE card via radiation-hard optical links called Versatile Twin-Transmitters (VTTx modules). These optical links operate at an impressive 5 GB/s between the front- and back-end systems.

Additional components of the QIE cards include the digital humidity and temperature sensor and the Bridge FPGA, the hub through which all of the QIE card's I^2C devices—the QIE11s, IGLOO2, VTTx modules, and humidity and temperature sensor chief among them—are accessed.

3.2 Test Stand Setup

For this HE front-end electronics upgrade, the Baylor high energy physics group collaborated with colleagues from the University of Minnesota, the University of Alabama, and the Florida Institute of Technology. As a team, we commissioned three test stands for initial inspection, quality control, and calibration of the QIE cards. All told, we tested 732 cards in a robust and manually intensive setup, aided by Python scripts and GUIs designed in-house.

3.2.1 Visual Inspection and Firmware

When shipments of QIE cards arrived at Fermilab from the manufacturer, we first inspected each card by hand for obvious manufacturing defects, such as bent components or incomplete soldering. We then probed the voltage rails that connect the cards to the low voltage supply, inspecting for shorts (Figure 3.4). If the hardware was physically intact, the card acquired a barcode sticker, allowing the card to be tracked throughout testing in the online database written specifically for the HE front-end electronics upgrade. Following this step, the two FGPAs—the Bridge and IGLOO2—were programmed with the most recent firmware using FlashPro software, and the VTTx housing was manually installed.

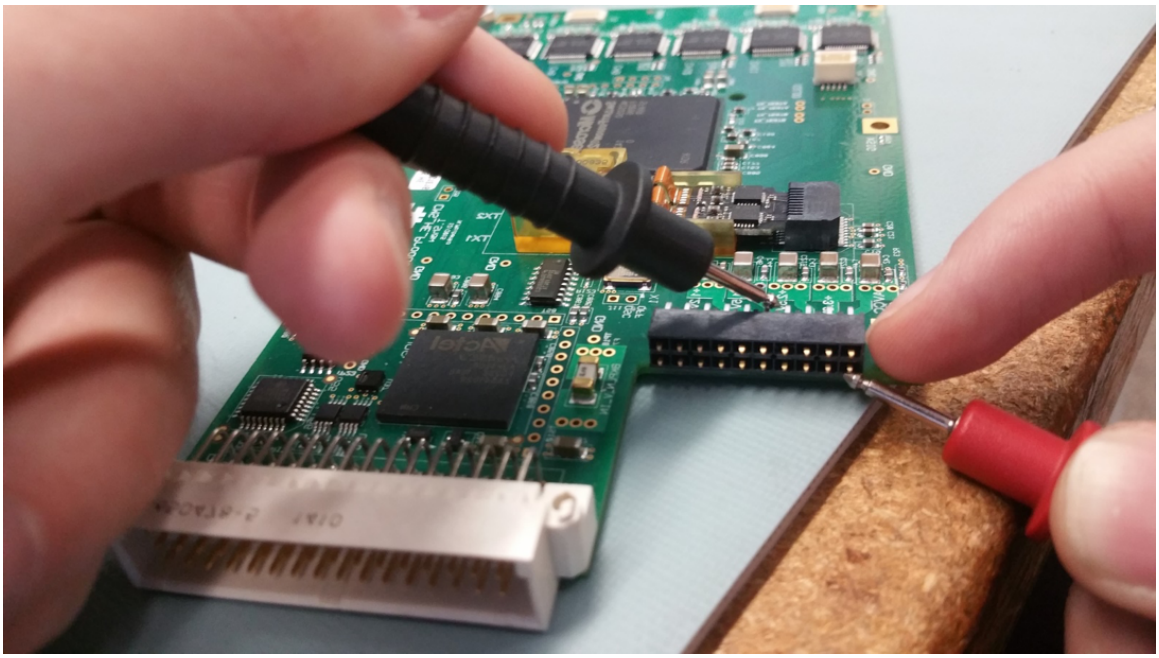

Figure 3.4. Probing the voltage rails of a QIE card at the first test stand.

3.2.2 Quality Control Testing

The Quality Control (QC) station required the most significant amount of coding collaboration. This test stand, along with the calibration station, arranged the electronics chain to mimic parts of HE. One of our Baylor students wrote the software for a server hosted by the versatile computer technology Raspberry Pi. We then accessed the local desktops in the lab and communicated with the Pi using ethernet. Thus the Pi acted as a liaison between the user commands and the fanout board, a circuit board designed for these test stands and equipped with a multiplexer to determine which electronic component receives instructions.

Wires ran from the fanout board to the ngCCM emulator, or the "next generation control-clock module," which occupies 4 slots out of 26 on the backplane (Figure 3.5). These ngCCM control and clock cards provide a good quality clock and orbit signal to the electronics as well as utilize the I^2C protocol. These functions allow robust synchronization of data across devices.

Figure 3.5. The four cards constituting the ngCCM emulator unit, designed by Baylor postdoc Joe Pastika.

Figure 3.6. A "full" backplane for the purposes of QC testing: 16 QIE cards, 2 ngCCM emulator control cards, and 2 ngCCM emulator clock cards.

In the QC testing, we filled 16 additional slots on the backplane with QIE cards for optimal testing efficiency (Figure 3.6). The Calibration Unit (CU) and SiPM control card slots were left open.

Properly programmed QIE cards should be able to receive and analyze data— such as analog pulses from the SiPMs— at the orbit speed of the LHC: 40 MHz. To ensure the performance of crucial internal functions of a card's components, we wrote a software test suite in the language Python. The tests communicated with each of the main components on the QIE card via the I^2C protocol.

The Python scripts were executed from several GUIs designed by a student at the University of Alabama. The scripts focused not only on accuracy and agreement with expected values, but also on consistency in a devise's response. Several factors such as LHC parameters, timed length of the test, and known margins of error affected the exact specifications for accuracy and consistency. Much of my code was focused on validating information stored in the IGLOO2 registers. For instance, the major and minor firmware versions for the IGLOO2 FPGA are stored as bits within a register, and it was essential that these versions were up-to-date and uniform across all 700 cards. Additionally, the internal input spy buffer could be analyzed to determine if proper capacitor rotation was occurring within QIE chips and if ADC and TDC values were within the legal range. The script also verified that read-only registers could not be overwritten and that read-write registers could be manipulated. I also wrote scripts to access and trigger on live humidity and temperature readings, adjust the shunt settings of QIE chips and manage charge injection plots, and verify proper registers and communication with the VTTx modules.

3.2.3 Calibration Testing

The final step in the testing efforts at Fermilab was calibrating the individual cards. To reach the calibration stage, the physical hardware, FPGA firmware, and performance of the QIE card components had to be assured via inspection and QC

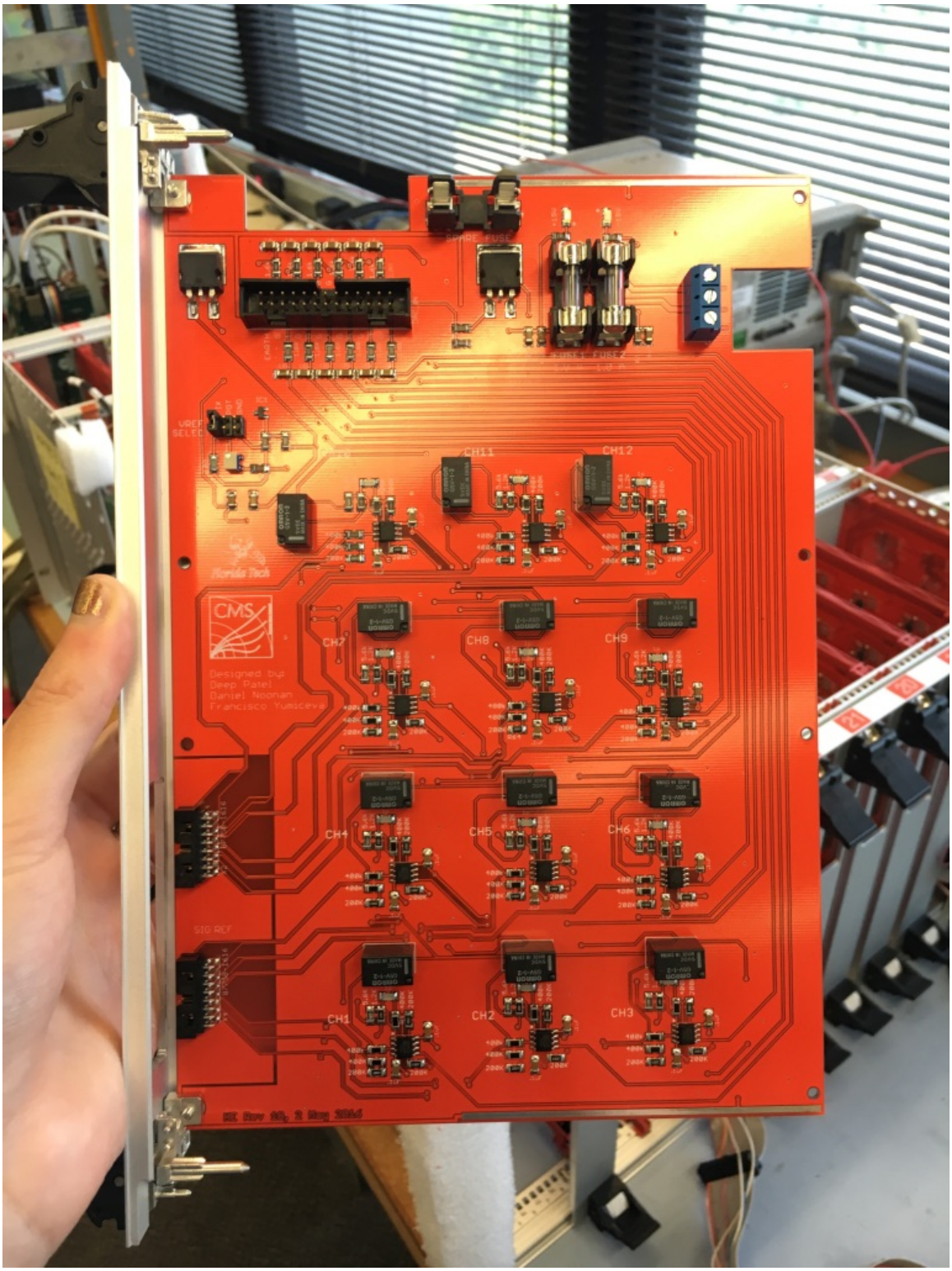

Figure 3.7. One charge injector (QI) card, with 12 distinct channels available. A completed charge injection crate holds 8 QI cards and a DAC unit.

testing. Before shipment to CERN, cards underwent extensive charge injection tests to log calibration data on each card's pedestal and shunt settings as well as overall response to current pulses.

As the first step in this process, charge injector (QI) cards and a crate layout were designed by the Florida Institute of Technology. To perform the actual calibration, we ran scripts enabling charge-injection mode on the QIE cards, a setting which could be verified by accessing the appropriate IGLOO2 register. Then the QI cards, controlled by a standalone Digital-to-Analog Converter (DAC), supplied DC current to the QIE cards to simulate a pulse arriving from SiPMs. Scripts scanned over the DAC and QIE11 internal shunt settings while we measured the ADC response.

I was intensely involved in the assembly and commissioning of the calibration test stand. Each red QI card has 12 relays (Figure 3.7), each of which corresponds to a channel—or a QIE11 chip—on a QIE card. Thus, the ideal setup involves a "full" backplane of 16 QIE cards attached to two charge injection crates containing 8 QI cards apiece. Since the QIE cards were designed to attach to custom flexible printed circuit boards and SiPM modules, a special setup was required to connect the QIEs to the charge injectors. Thin adaptor boards were secured to the tops of the QIE cards after successful completion of the QC station, and these boards then communicated with the QI cards via shielded ribbon cables (Figure 3.8).

The calibration station faced many challenges in both the commissioning and testing stages. The high number of electrical connections between devices, the length of the ribbon cables, and challenges with proper grounding contributed significantly to noise. Furthermore, retrieving the actual data from tests proved challenging within itself, with frequent failed communication between the test stand and the buffer and trigger system called the μHTR.

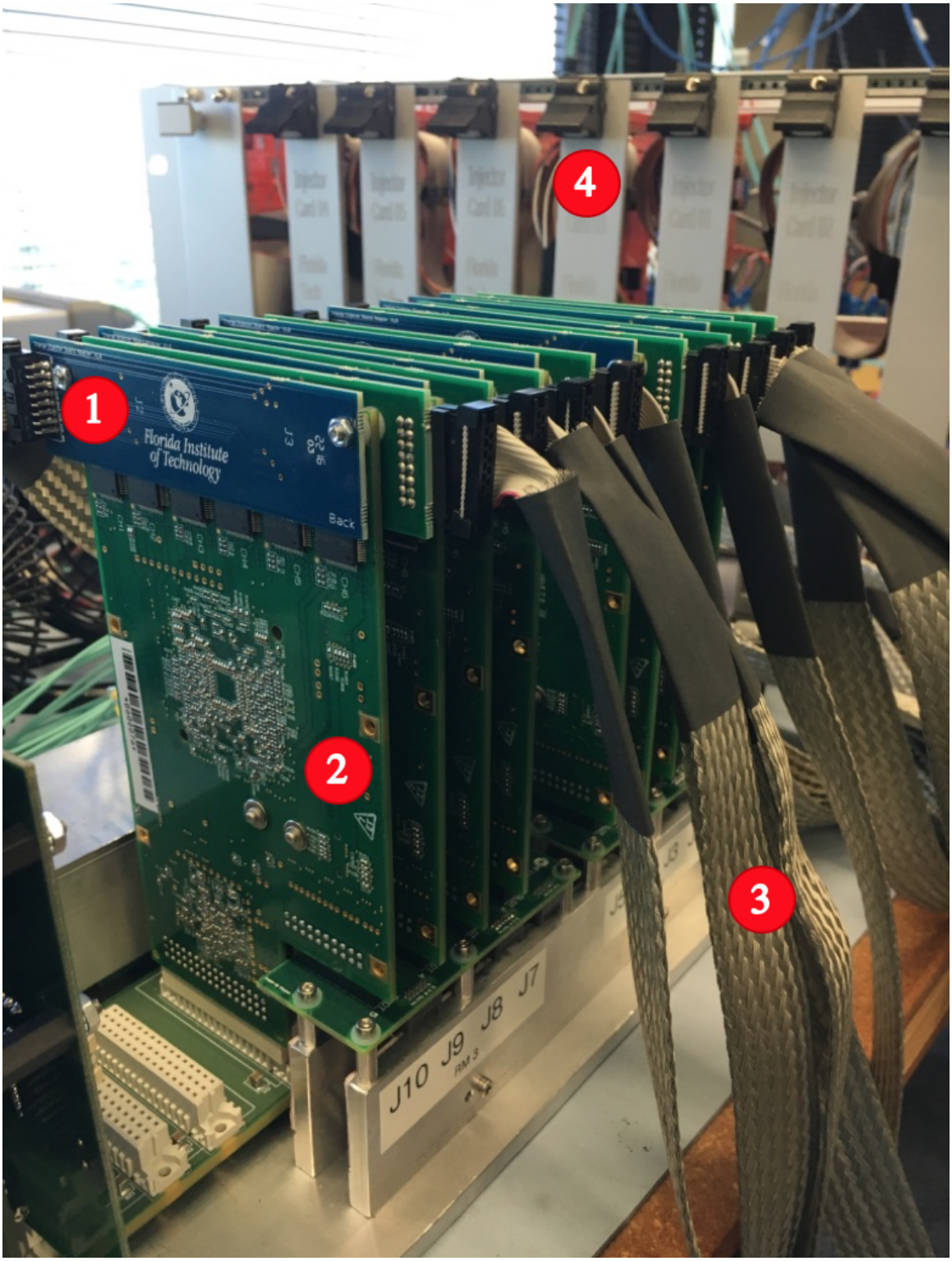

Figure 3.8. The charge injection station: 1) special adaptor board; 2) QIE card; 3) shielded ribbon cable; 4) QI card slotted into crate

CHAPTER FOUR

Results and Conclusions

4.1 The Dust Settles

The commissioning of the HE front-end electronics was merely one step in a massive, internationally-coordinated sequence for the HCAL upgrade. The HCAL project schedule was accelerated with the goal of squeezing the HE upgrade into the technical stop of Winter 2016–17. Our contribution of testing post-production electronics began in June 2016 and concluded in mid-August 2016. Despite the delays and troubleshooting at the calibration stage, we managed to complete card testing within the designated window (Figure 4.1), shipping them to CERN for assembly into readout boxes (RBXs), an arrangement including 16 QIE cards, 4 SiPM control cards interfaced with 4 arrays of 48 SiPMs, and a calibration unit.

The purpose of the calibration test stand was to obtain characteristic response data for each QIE chip on a card. This step allows for corrections to be made to the output from each card without necessitating complete homogeneity across all cards. Examples of the plots produced at the end of Summer 2016 for calibration data on hundreds of QIE cards' shunt settings are provided in Figure 4.2. Raw data for a single chip's ADC response is given in Figure 4.3.

4.2 Current Status of HE Upgrade

The deadlines were nominally met, but as December 2016 neared, the full breadth of the upgrade was placed on hold and a new plan—"Plan 1"—was drafted. Plan 1 eponymously called for the installation of one full RBX as a trial while the other RBXs undergo more testing. For ease of access for technical teams, this RBX has been installed in the 17th wedge out of 18 on the "plus" end of HE (labeled "HEP17"). On the "minus" side, 18 additional wedges hold the pre-upgrade electronics. Thus

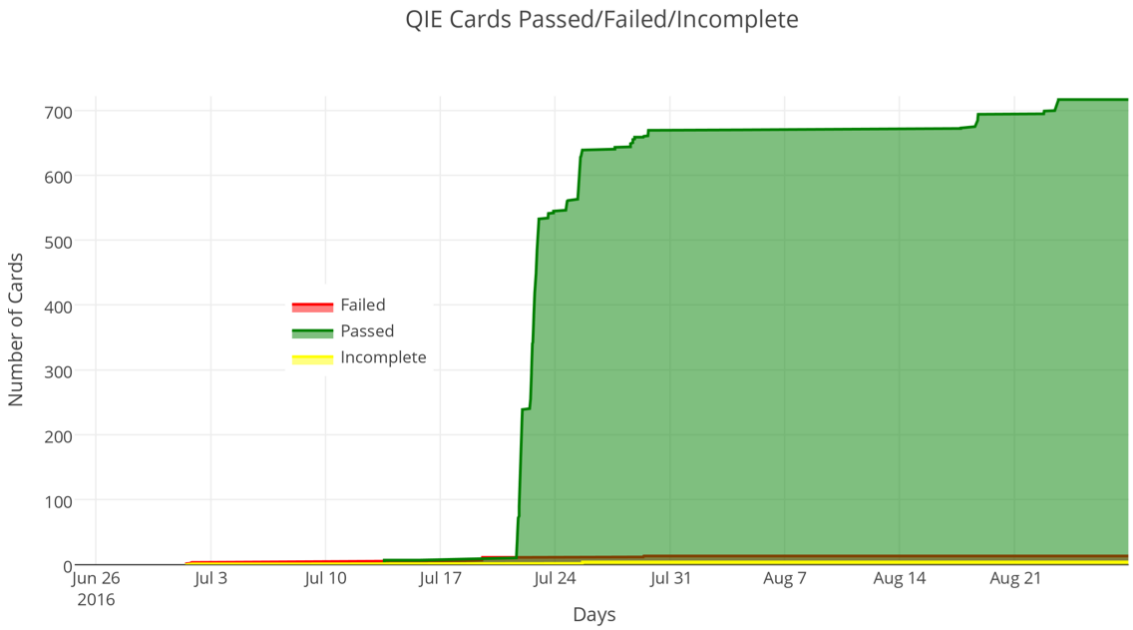

Figure 4.1. The cumulative number of QIE cards that passed all stations as a function of days during Summer 2016. Approximately 96% of cards were successful. The plot is generated and automatically updated in the online database for the HE front-end electronics upgrade.

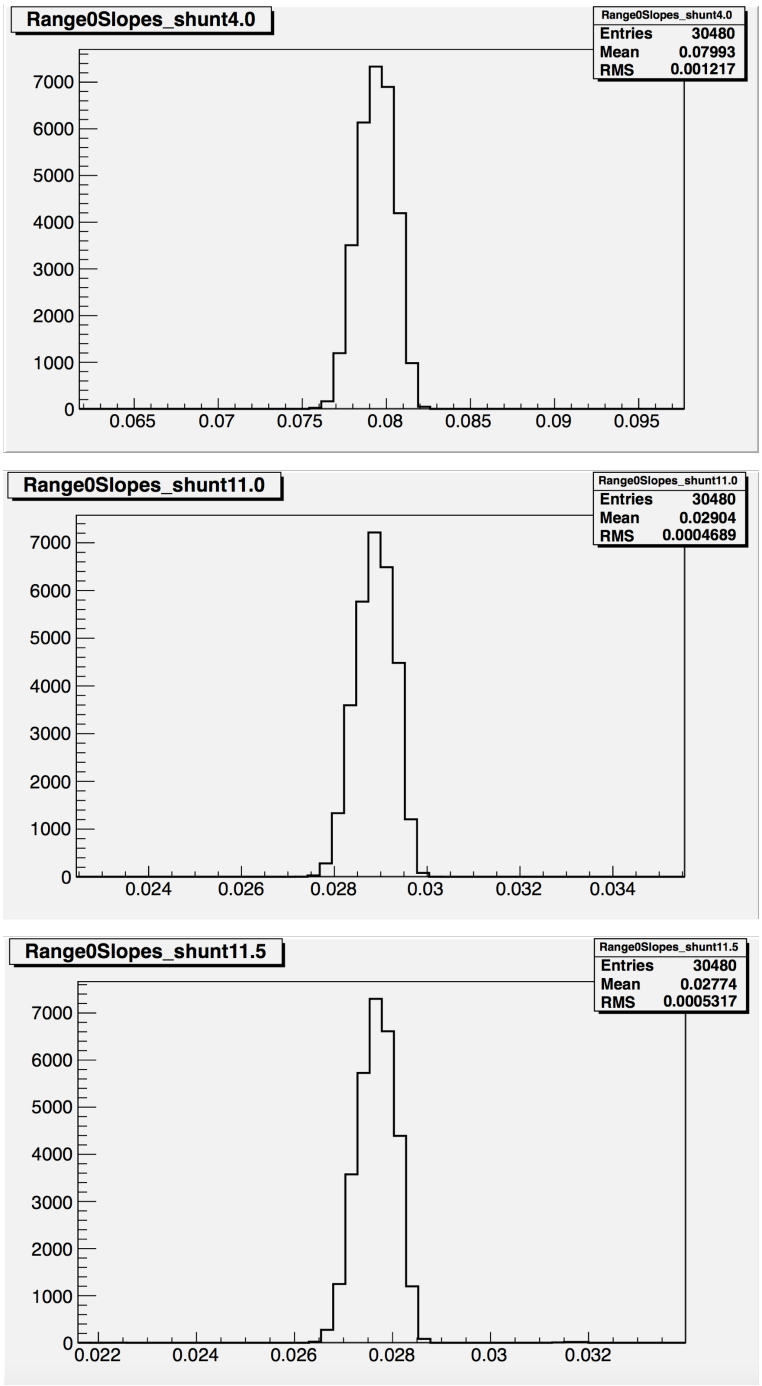

Figure 4.2. Histograms displaying the results of shunt tests for 635 QIE cards (635 $\times$ 12 QIE chips $\times$ 4 capacitors per chip = 30480 entries). Analyzing shunt settings was a principal test for calibration. Charge was injected into the chips as their internal shunts were raised, directly affecting the gain. Notice as the shunt setting increases from 4.0 to 11.0 to 11.5, the central value (response slope) decreases, which is as expected.

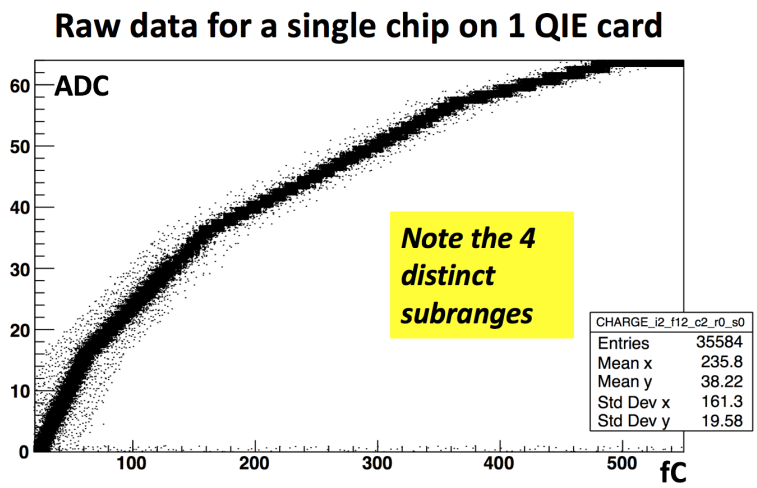

Figure 4.3. Raw data of ADC count (0–63) vs. charge in fC. Data is for Range 0 of a single chip on a QIE card. The calibration test stand was affected by noise, particularly evident here.

certain symmetries of the detector geometry are broken by the 35-to-1 ratio in the front-end RBXs. To avoid unnecessary strain on subsequent analyses reliant on the HCAL readout, current efforts are focused on calibrating and normalizing HEP17 data to match that of pre-upgrade QIEs and photodetectors. Run 2 of the LHC will proceed with this current hardware configuration until the next technical stop in Winter 2017-18, during which the whole of HE's front-end electronics is expected to be upgraded.

After the successful installation of HEP17, the commissioning process continued with "sourcing" (Figure 4.4). In order to gauge the response between scintillator layers and hardware, a radiating Cobalt-60 source was slowly fed through the material and the movement of the signal was tracked. In order to test the stability of the RBX itself as well as the communication links between the front- and back-end electronics such as the μHTR, laser tests between the calibration units (CU) and quartz fibers were also performed, verifying the mapping scheme.

In addition to these developments, the calibration process has extended into the spring of 2017 due to anomalous features particularly in the "offset" distributions

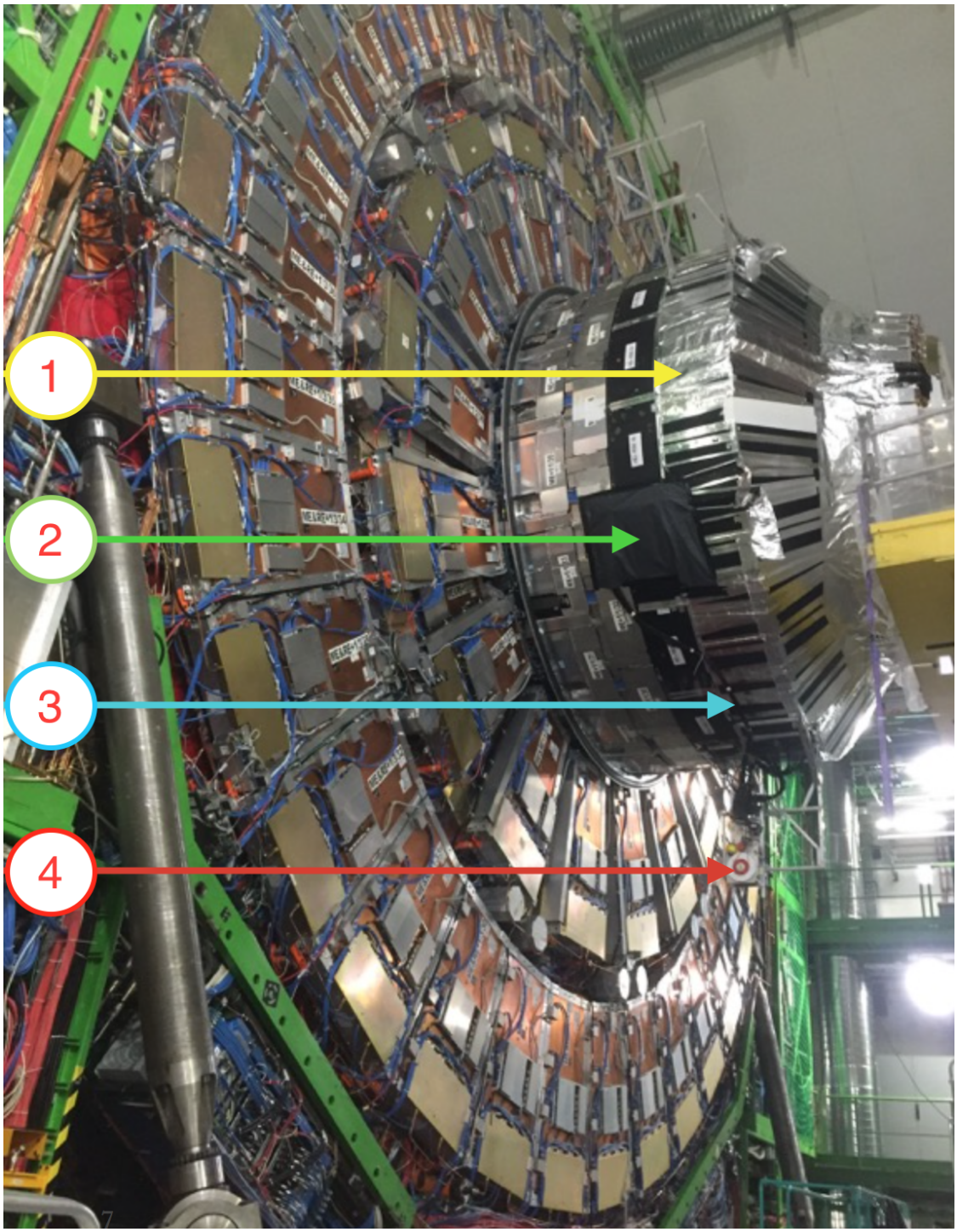

Figure 4.4. A view of the actual CMS detector in the midst of Plan 1 commissioning. 1) HCAL endcap; 2) the single RBX installed during the technical stop of Winter 2016–2017, located at "HE Plus 17," one of 18 wedges around the "plus" side of HE; 3) source tubes through which Cobalt-60 travels during sourcing tests; 4) source driver

of the QIE11s. To aid data fitting, linearized ADC units are used, and this linearized ADC is plotted versus fC total charge (pedestal + charge injection). The slope indicates the ADC bin width of each QIE11 chip. The un-shunted slopes and offset measurements from these recent tests are provided in Figure 4.5. Work is ongoing to account for the unexpected behavior in these distributions. As seen in Figure 4.6, the slopes for shunted QIE11s indicate appropriate performance in the HEP17 cards. Overall, preliminary results from Plan 1 indicate promising improvements in HE performance as well as offer a strong proof-of-concept for the full upgrade of front-end electronics.

The project has helped ensure that HCAL readout is stable and well-understood across all major components, and all signs indicate that the envisioned HE upgrade will be a successful and appropriate way to respond to the challenges of signal loss and high luminosity. As a result of these studies and the efforts of countless collaborators across dozens of institutions, more precise hadronic measurements will be produced at high energy scales. The better collision data that follow will guide researchers as they continue testing models against empirical data in this stratospheric energy sector and as they pursue a collaborative spirit on the frontiers of knowledge.

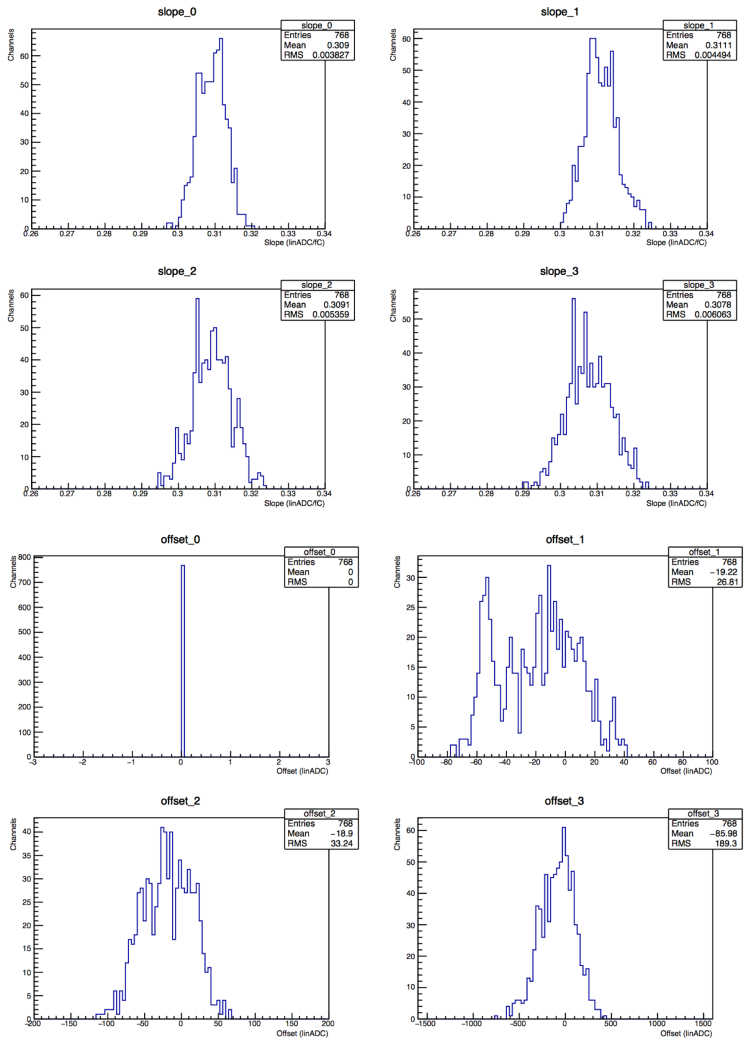

Figure 4.5. The top four histograms demonstrate the calibration slope values obtained from range 0–3 of the 16 QIE cards at HEP17. The distribution is acceptable. The lower four histograms indicate that the "offset"—a measurement intimately related to the pedestal values of the QIE11 and QI card—is not properly measured [5].

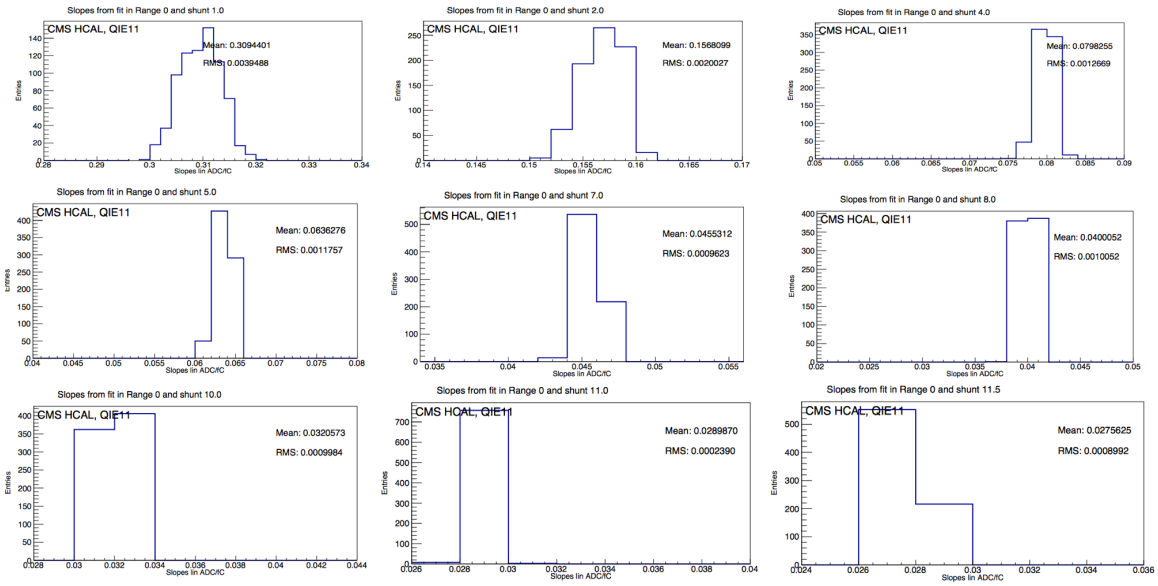

Figure 4.6. Histograms for the calculated slopes for each shunt setting on HEP17 QIE11 chips. Note that as the shunt setting increases by an order of magnitude from 1.0 up to 10.0, the mean slope value decreases by an order of magnitude. This change reflects the underlying nature of the shunt-gain relationship. Furthermore, note that the number of bins in each histogram roughly decreases by a factor of ten as well, indicating the less granulated binning that occurs for higher shunts [6].

BIBLIOGRAPHY

[1] Matter-Energy Conversion.
http://www.alternativephysics.org/book/MatterEnergy2.htm.

[2] T. Khurshid. *Detector Control System for CMS Endcap RPCs*. Ph.D. Thesis, Quaid-I-Azam University, September 2015.

[3] L. Mastrolorenzo. *Search for the Higgs boson decaying into τ lepton pairs with the Matrix Element Method and τ trigger optimization in the CMS experiment at the LHC*. Ph.D. Thesis, École Polytechnique, Paris-Saclay University, October 2015.

[4] E. Hughes. A New Integrated Circuit for the Upgrade HCAL Front-End.
https://indico.cern.ch/event/276484/#3-phase-i-upgrade-of-the-hcal.

[5] D. Noonan. HE QIE11 Calibration, March 2017.
https://indico.cern.ch/event/618021/#68-qie-calibration-report.

[6] T. Roy, D. Noonan, and F. Yumiceva. HE Calibration, March 2017.
https://indico.cern.ch/event/623885/#68-qie-calibration-report.

[7] A. Drager. *Prediction of the $t\bar{t}$ and W + Jets Background in a Search for New Physics with Jets and Missing Transverse Energy at CMS*. Ph.D. Thesis, Hamburg University, February 2016.

[8] The HL-LHC Project: LHC baseline.
http://hilumilhc.web.cern.ch/about/lhc-baseline.

[9] J. Garcia. *Search for Higgs-Boson Production in Association with Top-Quark Pairs in $H \to b\bar{b}$ Decays at $\sqrt{s}$ = 8 and 13 TeV with the CMS Experiment*. Ph.D. Thesis, Hamburg University, June 2016.

[10] The Accelerator Complex. https://home.cern/about/accelerators.

[11] J. Hirschauer. HE Front End Production Status, 2016.
https://indico.cern.ch/event/548010/#2-he-fe-production-status-qie1.

[12] J. Pastika. HCAL DAQ Overview, 2016.
https://indico.cern.ch/event/523873/#4-introduction-to-readout-elec.